Rare Metal Materials and Engineering
Volume 51, Issue 10, October 2022
Available online at www.rmme.ac.cn

Science Press

Cite this article as: Mei Jinna, Han Yaolei, Peng Qunjia, et al. Effects of Wear on Stress Corrosion Cracking Initiation Behavior of Alloy 690 Steam Generator Tubes[J]. Rare Metal Materials and Engineering, 2022, 51(10): 3547-3553.

ARTICLE

Effects of Wear on Stress Corrosion Cracking Initiation Behavior of Alloy 690 Steam Generator Tubes

Mei Jinna, Han Yaolei, Peng Qunjia, Cai Zhen, Wang Peng, Ti Wenxin

Suzhou Nuclear Power Research Institute, Suzhou 215004, China

Abstract: Tube bundles are the most critical components of steam generators in pressurized water plants. They are the heat exchange interface between primary and secondary circuits, acting as an important safety barrier to prevent the radioactive leakage. Stress corrosion cracking (SCC) initiation behavior of the worn alloy 690 tubes was investigated by slow strain rate tests (SSRT) in the high-temperature alkaline solution. The scanning electron microscope, electron backscatter diffraction and transmission electron microscope were used to analyze the fretting wear and SCC initiation behavior of alloy 690 tubes. Results show that SSRT specimens show typical transgranular SCC characteristics. The number of initiated cracks and their average depth are increased with increase in the wear degree, suggesting a wear-induced SCC initiation. This may have a relationship with the grooves, delamination, micro-cracks and residual strain layer with tens of micrometers in thickness left on the worn surface. Furthermore, a preliminary analysis on the possible procedure of wear-induced SCC initiation and further propagation during SSRT tests was carried out based on slip-dissolution/oxidation mechanism.

Key words: nickel-base 690 alloy; high-temperature alkaline solution; wear; stress corrosion cracking

Steam generator (SG) is one of the key equipments in the nuclear power plants, which is used to transfer the heat in the reactor coolant circuit to the secondary side water, and further to generate saturated steam for the secondary circuit power device. Tube bundles are the most critical components of SG. On the one hand, they are the heat exchange interface between primary and secondary circuits. On the other hand, the pressure boundary area of SG tube bundles accounts for about 80% of the total area of the primary pressure boundary, acting as an important safety barrier to prevent the radioactive leakage. Reactor coolant containing boric acid and lithium hydroxide, and weak alkaline solution containing ammonia and diamine are in the primary side and secondary side of SG tubes, respectively. Under the normal operation condition, the temperature and pressure in the primary side and secondary side of SG tubes are 293~327 °C, 15.5 MPa and 226~283 °C, 8.6 MPa, respectively.

SG tubes used in nuclear power plants are found to be susceptible to fretting wear[1-7] and stress corrosion cracking (SCC)[8-17]. The SCC is a synergic effect of material, mechanics and environment, which are directly related to the material surface state such as scratches[18-23]. The fretting wear between the SG tube and the anti-vibration bar (AVB) or the tube support plate (TSP) caused by flow-induced vibration is unavoidable, which consequently causes a lot of defects on the surface, and leads to the initiation of SCC. Alloy 690 is used frequently as the SG tube material. As such, investigation on the effects of fretting wear on the SCC of alloy 690 is helpful to clarify the mechanism of the SCC initiation of the steam generator tubes.

In this study, the slow strain rate tensile test (SSRT) method was used to investigate the effects of wear on the SCC initiation behavior of alloy 690 tube in high-temperature alkaline solution. The wear and SCC behavior were revealed by characterizing the surface state and the cracks formed during the SSRT. The correlation between the wear and SCC was discussed.

Received date: October 15, 2021
Foundation item: Natural Science Foundation of Jiangsu Province (BK2018117, BK20180210); Scientific Research and Innovation Project of China General Nuclear Power Group (3100129119); National Science and Technology Major Project of China (2019ZX06005003)
Corresponding author: Mei Jinna, Ph. D., Professor, Suzhou Nuclear Power Research Institute, Suzhou 215004, P. R. China, Tel: 0086-512-83552387, E-mail: meijinna@cgnpc.com.cn

1 Experiment

Commercial alloy 690 tubes with an outer diameter of 19.05 mm and a wall thickness of 1.09 mm were used for the fretting wear and SCC tests. The chemical composition of alloy 690 is listed in Table 1. Specimens were cut from the as-received materials.

X6Cr13 AVB specimens with a dimension of 34 mm×12.5 mm×3.5 mm were used as the contact material to alloy 690 tubes in the fretting wear test. The illustration of fretting wear between the alloy 690 tube and X6Cr13 AVB is shown in Fig.1. The vertical reciprocating relative friction movement of X6Cr13 AVB sheet against alloy 690 tube under the normal force was performed during the fretting wear test in deionized water at room temperature, in order to get fretting wear damaged alloy 690 tube specimens for the subsequent slow strain rate tensile tests. Fretting wear tests were performed under the displacement amplitude of 200 μm with a frequency of 20 Hz until the wear depth ratio of 20%, 40% and 60% (the ratio of wear depth to the tube wall thickness) were obtained. Alloy 690 tubes were cleaned ultrasonically in ethanol after the fretting wear tests. The worn surface morphology was observed by a TESCAN VEGA 5136XM scanning electron microscopy (SEM), and the residual strain of the worn surface was measured using a ZEISS Sigma 300 SEM equipped with electron backscatter diffraction (EBSD) in connection with the Channel 5 software. A step size of 0.5 μm at a voltage of 25 keV was used in the EBSD residual strain analysis. The microstructure of the cross-section specimen along the depth direction was observed by a Tecnai G2 F20 S-TWIN transmission electron microscope (TEM) equipped with an energy dispersive X-ray spectroscopy (EDS). The TEM specimens were prepared by a FEI-Scios focus ion beam (FIB) system.

SCC behavior of the alloy 690 tube specimens was tested at a strain rate of 1×10^{-6} s^{-1} in a 10wt% sodium hydroxide alkaline solution at 290 °C (7.5 MPa) by simulating the secondary side water on a SERT-5000DP-9L tensile testing machine (TOSHIN KOGYO Co., Ltd, Japan) equipped with a static autoclave. The alkaline solution was prepared using high purity water and NaOH (99wt%). The dissolved oxygen (DO) in the alkaline solution was controlled at <5 μg/L by introducing the high-purity nitrogen gas for 3 h. Characterizations of the cracks formed on alloy 690 tubes were then conducted to clarify the SCC behavior. The surface morphology of each specimen was observed using the SEM. Then each specimen was sliced into three pieces along the longitudinal direction for counting the number of cracks and measuring the depth of cracks on the cross-section of the specimens within a distance of 1 mm near the fracture. To reveal the characteristics of the grain boundary near the cracks, electron backscatter diffraction (EBSD) analysis was conducted with a step size of 0.5 μm at a voltage of 20 keV using a ZEISS Sigma 300 SEM equipped with a camera in connection with the TSL software. Specimens for the EBSD analysis were prepared through grinding mechanically by SiC papers up to 2000 grit, polished by a diamond paste of 1 μm and the 40 nm colloidal silica slurry successively.

Table 1 Chemical composition of alloy 690 tube (wt%)

Cr	Fe	Mn	Ti	S	P	C	Si	Cu	Al	Ni
29.31	10.26	0.31	0.25	0.002	0.009	0.025	0.11	0.04	0.39	Bal.

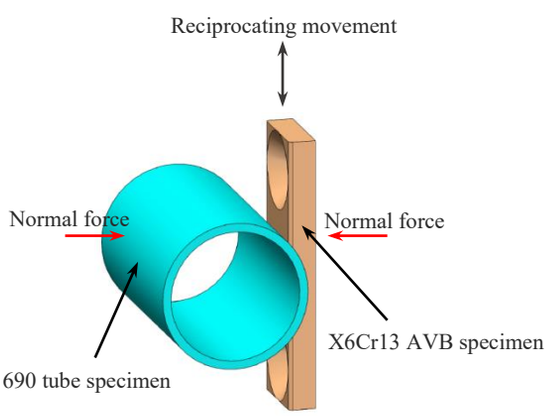

Fig.1 Illustration of fretting wear between alloy 690 tube and X6Cr13 AVB

2 Results and Discussion

2.1 Results

Fig.2 shows the typical SEM images of the worn surface of alloy 690 tube specimen with a wear depth ratio of 40%. A mixed characteristic of grooves and delamination as well as a few microcracks can be observed, revealing a complicated fret-ting wear mechanism of abrasive wear and delamination

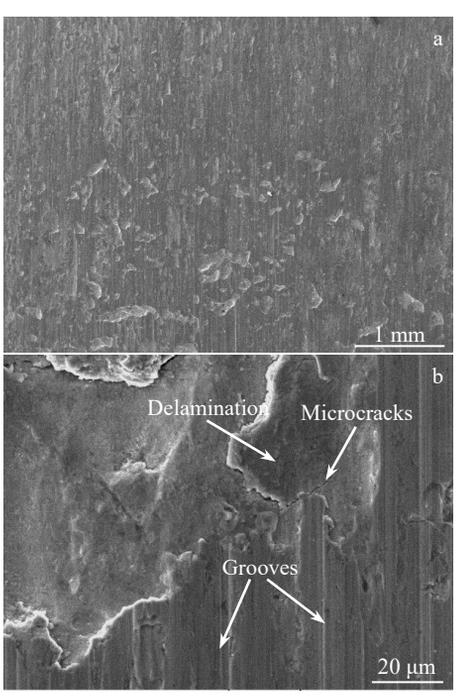

Fig.2 SEM images of worn surface of alloy 690 tube specimen with a wear depth ratio of 40%: (a) 50× and (b) 2000×

wear.

Fig.3 shows the EBSD observation of the strain layer on the cross-section of the worn area of alloy 690 tube specimen with a wear depth ratio of 60%. The red and yellow areas reveal a rather higher residual strain, while the blue areas show a less residual strain. The thickness of the residual strain layer can be accordingly measured to be about 10 μm near the worn surface.

Fig.4 shows the TEM image of the wear center area of the alloy 690 tube specimen with a wear depth ratio of 60%. A large amount of dislocations and slips that are accumulated beneath the worn area can be observed obviously, indicating a severe plastic deformation induced by fretting wear.

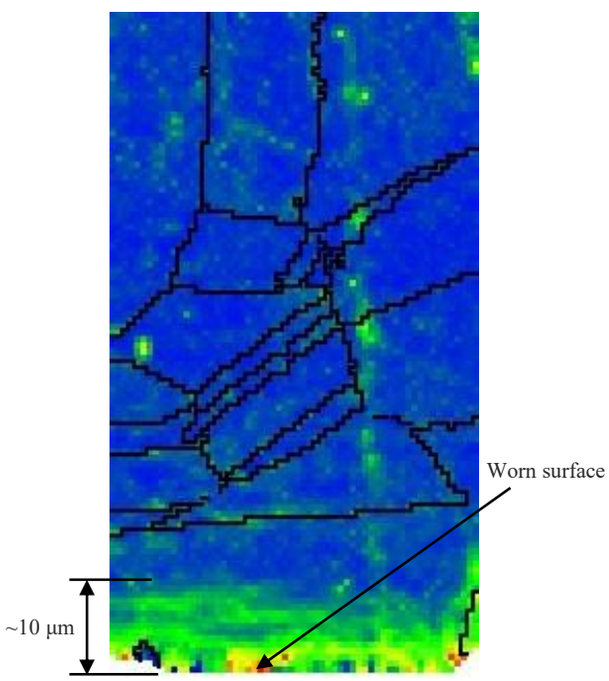

Fig.3 EBSD observation of cross-section of alloy 690 tube specimen with a wear depth ratio of 60%

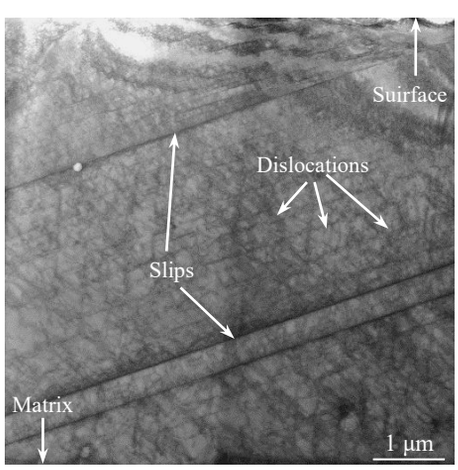

Fig.4 TEM image of microstructure of the worn area on the alloy 690 tube specimen with a wear depth ratio of 60%

The load-displacement curves for SSRT of unworn and worn alloy 690 specimens with different wear depth ratios are shown in Fig. 5. The maximum loads obtained from the load-displacement curves are listed in Table 2. It is found that the maximum load of alloy 690 specimens decreases significantly from 4018 N to 2117 N with increase in wear depth ratio from 0% to 60%.

The morphologies of worn area near the fracture of alloy 690 SSRT specimens with different wear depth ratios are shown in Fig. 6. It is found that the surface of unworn specimen is covered with Fe-Ni-Cr oxides with a size less than 10 μm. Some micro cracks on the surface of alloy 690 specimen with a wear depth ratio of 20% perpendicular to the tensile stress direction are observed. The cracks become denser and the size of the cracks becomes larger, when the wear depth ratio increases from 20% to 60%.

Fig.7 shows the longitudinal cross-section morphologies of worn area near the fracture of the alloy 690 specimens with wear depth ratios of 0%, 20%, 40% and 60% after SSRTs. The cracks with a depth of 5~15 μm can be observed on the unworn specimen and worn specimen with wear depth ratio of 20%. The number and the average depth of the initiated cracks increase with further increase in the wear depth ratio from 20% to 60%. In order to clarify the characteristic of cracks, EBSD analysis for longitudinal cross-section of the worn area near the fracture of alloy 690 tube specimens with different wear depths was performed. Fig. 8 shows a typical image of the cracks detected by EBSD for the specimen with a wear depth ratio of 60%, revealing obvious transgranular SCC characteristics.

The statistical results of the number of cracks with different

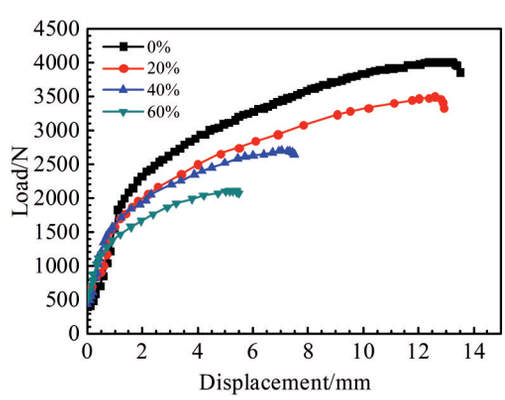

Fig.5 Slow strain rate tensile curves of alloy 690 specimens with different wear depth ratios in the high temperature alkaline solution

Table 2 Maximum load for SSRT of alloy 690 specimens

Ratio of wear depth to tube wall thickness/%	Maximum load/N
0	4018
20	3508
40	2705
60	2117

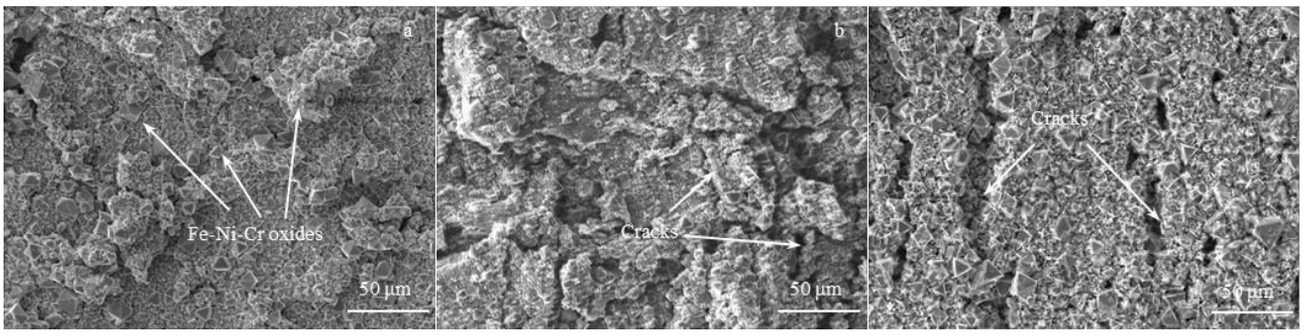

Fig.6 Surface morphologies of worn area near the fracture of alloy 690 specimens with different wear depth ratios after SSRT: (a) 0%, (b) 20%, and (c) 60%

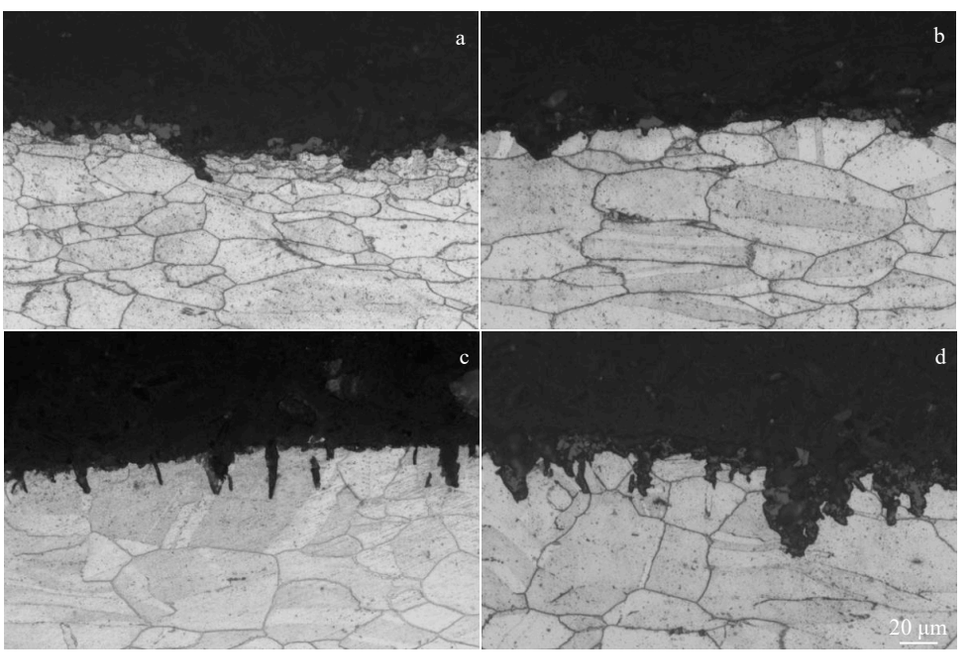

Fig.7 Longitudinal cross-section morphologies of worn area near the fracture of alloy 690 specimens with different wear depth ratios after SSRT: (a) 0%, (b) 20%, (c) 40%, and (d) 60%

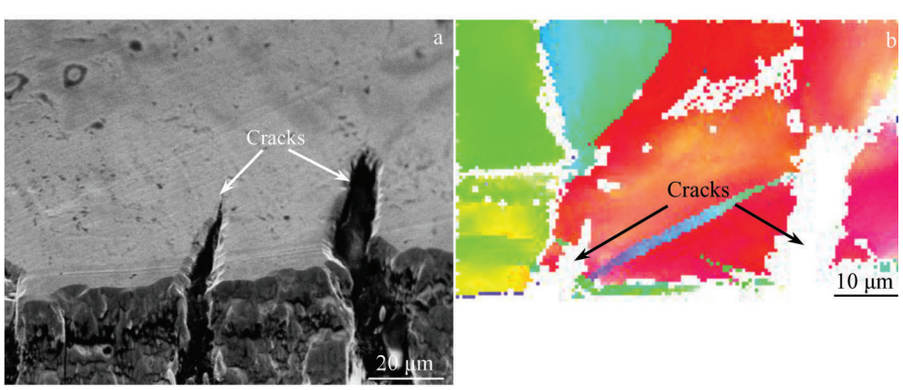

Fig.8 SEM image (a) and EBSD observation (b) of longitudinal cross-section of the worn area near the fracture of alloy 690 specimen with a wear depth ratio of 60%

depth observed on the longitudinal cross-section specimens with wear depth ratios of 0%, 20%, 40% and 60% are summarized in Fig.9. The corresponding maximum depth and average depth of cracks are listed in Table 3. The total number of cracks of the longitudinal cross-section specimens with wear depth ratios of 0%, 20%, 40% and 60% is 20, 18, 22 and

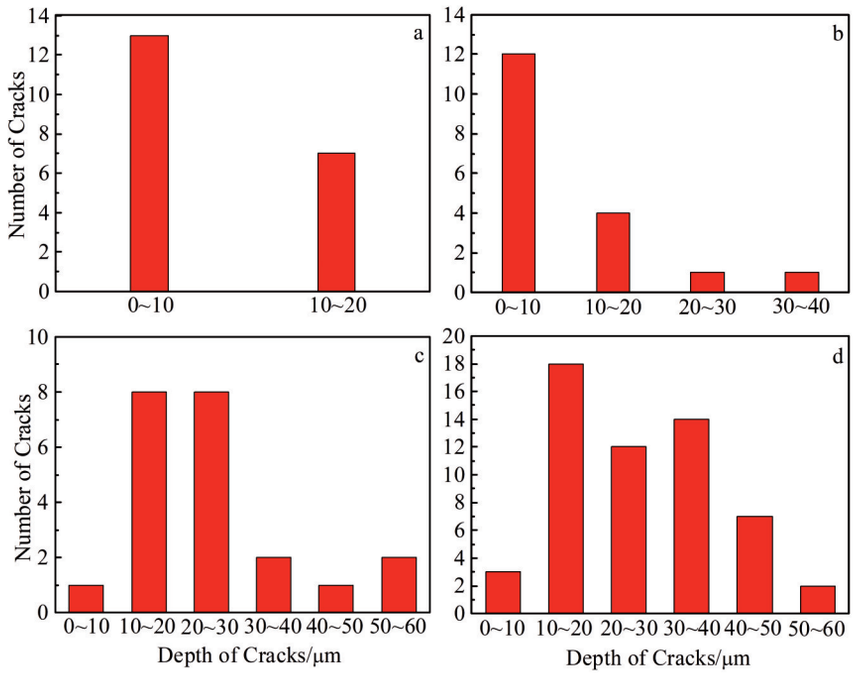

Fig.9 Number and depth of the cracks observed on the longitudinal section specimens with different wear depth ratios: (a) 0%, (b) 20%, (c) 40%, and (d) 60%

Table 3 Maximum depth and average depth of the cracks

Ratio of wear depth to thickness of tube wall/%	Maximum depth of cracks/μm	Average depth of cracks/μm
0	15.8	8.4
20	33.1	10.7
40	56.3	25.9
60	51.5	26.9

56, respectively, indicating an increase in the total number of cracks with increasing the wear depth. In addition, it is found that the unworn specimen shows the smallest maximum crack depth of 15.8 μm and the smallest average crack depth of 8.4 μm. The depth of most cracks is within 20 μm. The maximum depth and the average depth of the cracks show a rapid growth of 3 times with rising the wear depth ratio from 0% to 40%. The maximum depth and the average depth of the cracks reach the similar value with the increase of the wear depth ratio from 40% to 60%.

2.2 Discussion

The above results indicate that wear promotes the initiation of SCC, which is probably induced by the change of the surface state of material caused by fretting wear. Fig.10 shows the schematic diagram to illustrate the effect of wear on the SCC initiation of alloy 690 tube in a high-temperature alkaline solution. The alloy 690 tube surface is damaged severely during fretting, and a mixed characteristic of grooves and delamination as well as a few micro-cracks can be observed on the worn surface as shown in Fig. 2. This indicates the combined wear mechanism of abrasive wear and delamination wear[24,25]. In addition, EBSD and TEM results prove a residual strain layer with proximately 10 μm in thickness and a high level of residual stress under the wear surface as shown in Fig. 3 and Fig. 4. During the fretting wear process, abrasive wear occurs. The cyclic load is applied on the surface and subsurface of the specimens during the reciprocating wear process. This fatigue process leads to the accumulation of defects such as dislocations and stacking faults. Furthermore, the slips and even micro-cracks occur in the substrate due to the complex stresses mentioned above. Some micro-cracks are further propagated and combined, which finally causes the removal of material.

According to the slip-dissolution/oxidation mechanism, the surface state and the residual strain play important roles in the SCC initiation process[26,27]. When the surface of alloy 690 tube is destroyed by fretting wear, the number of the SCC initiation positions increases, such as the micro-cracks, the delamination and the grooves. Meanwhile, more dislocations in the deformation layer of the worn tubes move along the slip plane to form large slip steps, leading to the stress concentration on the worn surface under the applied stress. The surface oxide film near the slips exposed in high-temperature solution is broken and thus the new matrix metal is exposed to the high-temperature alkaline solution and dissolved. A passivation film will be formed again. The dislocations will slip and thus the oxide film will be broken again under the stress. This process is repeated over and over,

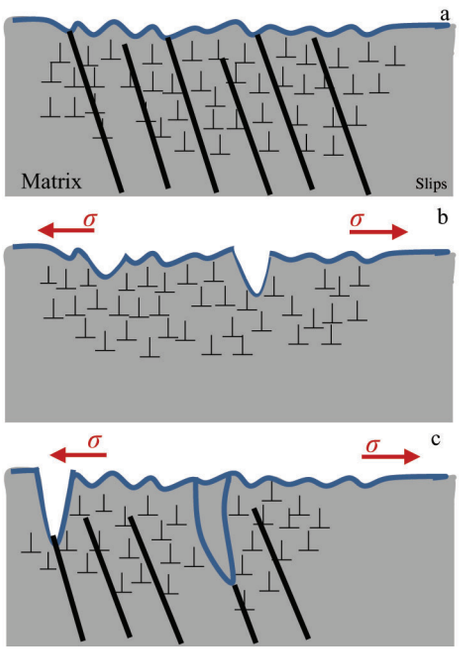

Fig.10 Schematic diagrams illustrating the effect of wear on the SCC of alloy 690 tube in a high-temperature alkaline solution: (a) worn surface, (b) SCC initiation, and (c) SCC propagation

causing cracks to grow. Accordingly, the cracks continue to propagate along the sliding steps to the inside of the matrix metal. The increase in the degree of wear leads to an increase in local stress concentration, which in turn promotes an increase in the number and depth of SCC initiation.

3 Conclusions

1) Alloy 690 tubes show a complex morphology after fretting wear, including grooves, delamination, micro-cracks, and residual strain layer with tens of micrometers in thickness.

2) Alloy 690 specimens with a wear depth ratio of 0%~60% after SSRT tests show the characteristic of predominant transgranular SCC.

3) The increased degree of surface damage and local stress concentration caused by wear promote the SCC initiation in high-temperature alkaline solution according to the slip-dissolution/oxidation mechanism.

References

1 Yun J Y, Shin G S, Kim D I *et al*. *Wear*[J], 2015, 338-339: 252

2 Guerout F M, Fisher N J. *Journal of Pressure Vessel Technology* [J], 1999, 121(3): 304

3 Fisher N J, Chow A B, Weckwerth M K. *Journal of Pressure Vessel Technology*[J], 1995, 117(4): 312

4 Lee Y H, Kim I S. *Wear*[J], 2002, 253(3-4): 438

5 Kong J K, Kim I S. *Wear*[J], 2003, 255(7-12): 1174

6 Lee Y H, Kim I S, Kang S S *et al*. *Wear*[J], 2001, 250(1-12): 718

7 Jeong S H, Cho C W, Lee Y Z. *Tribology International*[J], 2005, 38(3): 283

8 Dutta R S, Tewari R, De P K. *Corrosion Science*[J], 2007, 49(2): 303

9 Li Xiaohui, Huang Fa, Wang Jianqiu *et al*. *Acta Metallurgical Sinica* [J], 2011, 47(7): 847 (in Chinese)

10 Kuang W J, Was G S. *Corrosion Science*[J], 2015, 97: 107

11 Tang Z M, Meng F J, Zhang P Z *et al*. *Rare Metal Materials and Engineering*[J], 2019, 48(11): 3541

12 Park I G, Lee C S, Hwang S S *et al*. *Metals and Materials International*[J], 2005, 11: 401

13 Ahn S J, Rao V S, Kwon H S *et al*. *Corrosion Science*[J], 2006, 48(5): 1137

14 Xu Ying, Sun Baode. *Nuclear Power Engineering*[J], 1995, 16(05): 459 (in Chinese)

15 Memg F J, Wang J Q, Han E H *et al*. *Corrosion Science*[J], 2009, 51(11): 2761

16 Shoemaker C E, Cordovi M, Stein A A. *Workshop on Thermally Treated Alloy 690 Tubes for Nuclear Steam Generators: Proceedings*, EPRI-NP-4665M-SR[R]. Palo Alto: EPRI, 1986

17 Castano-Matin M L. *Proceedings of the 6th International Symposium on Environmental Degradation of Materials in Nuclear Power Systems -Water Reactors*[C]. San Diego: The Minerals, Metals & Materials Society, 1993

18 Staehle R W, Gorman J A. *Corrosion*[J], 2003, 59(11): 931

19 Zhao L Y, Cui Y H, Yang F Q *et al*. *Rare Metal Materials and Engineering*[J], 2018, 47(5): 1399

20 Sykes L J. *Analysis of Steam Generator Tubing from Oconee Unit 1 Nuclear Station*, TR-106484[R]. Palo Alto: EPRI, 1997

21 Kuchirka P J, Blaszkiewicz, Byers W A *et al*. *Oconee 2 Steam Generator Tube Examination*, TR-106863[R]. Palo Alto: EPRI, 1997

22 MacDonal P E, Shah V N, Ward L W *et al*. *Steam Generator Tube Failures*, NUREG/CR-6365[R]. Washington: NRC, 1996

23 Rochester D P. *Water Chemistry of Nuclear Reactor Systems*[M]. London: Thomas Telford Publishing, 2001

24 Chung I, Lee M. *Nuclear Engineering and Design*[J], 2011, 241(10): 4103

25 Lim M K, Oh S D, Lee Y Z. *Nuclear Engineering and Design* [J], 2003, 226(2): 97

26 Han Y L, Mei J N, Peng Q J *et al*. *Corrosion Science*[J], 2015, 98: 72

27 Han Y L, Mei J N, Peng Q J *et al*. *Corrosion Science*[J], 2016, 112: 625

磨损对蒸汽发生器690合金传热管应力腐蚀裂纹萌生行为的影响

梅金娜，韩姚磊，彭群家，蔡　振，王　鹏，逄文新
(苏州热工研究院有限公司，江苏 苏州 215004)

摘　要：传热管是蒸汽发生器（SG）最关键的部件，起到一、二回路换热的作用，是防止放射性泄漏的重要安全屏障。在高温碱性溶液中进行了磨损690合金传热管的慢应变速率拉伸试验（SSRT）。采用扫描电子显微镜、电子背散射衍射和透射电子显微镜分析了690合金传热管的微动磨损和应力腐蚀裂纹（SCC）萌生行为。结果表明，SSRT试样呈现出典型的穿晶SCC特征，且随磨损深度增加，裂纹萌生数量和平均深度均增加，这可能与磨损表面留下的犁沟、剥层、微裂纹以及数十微米厚的残余应变层有关。基于SCC的滑移溶解/氧化机制，对磨损促进SCC裂纹萌生的过程进行了分析。

关键词：镍基690合金；高温碱性溶液；磨损；应力腐蚀开裂

作者简介：梅金娜，女，1981年生，博士，教授级高级工程师，苏州热工研究院有限公司，江苏 苏州 215004，电话：0512-83552387，E-mail：meijinna@cgnpc.com.cn